Available online at www.sciencedirect.com
ScienceDirect
Journal of Computational Physics 227 (2008) 5758–5777
JOURNAL OF COMPUTATIONAL PHYSICS
www.elsevier.com/locate/jcp

A hybrid Boltzmann electrons and PIC ions model for simulating transient state of partially ionized plasma

Dixon T.K. Kwok *

APPG, School of Physics A28, University of Sydney, NSW 2006, Australia

Received 18 July 2007; received in revised form 5 February 2008; accepted 7 February 2008
Available online 16 February 2008

Abstract

A robust and stable numerical algorithm is developed for the hybrid method of particle-in-cell ions and Boltzmann distribution of electrons. A different approach to estimate the electron density reference and its proper potential reference is developed to overcome the problems of instability and divergence of previous approaches. The electron density reference is precisely calculated, the tolerance criterion is well-defined, and convergence is guaranteed by applying bi-section golden rule. To increase the rate of convergence, an external loop is incorporated with the bi-section golden rule to vary the brackets. The validity of the method is proved by comparing the simulated result with well-known analytical formula. The simulated sheath potential at a floating wall fit well to the analytic result. The collisionless ion kinetic energy acquired from the voltage difference between the pre-sheath and ion sheath does not violate the Bohm sheath criterion. For work that focuses on the plasma process at the ion sheath and not on the generation of plasma, this method saves simulation time by avoiding time consuming particle or kinetic model of electrons. The new approach reproduces the ion density profile at the ion sheaths region of a plasma with bi-Maxwellian electrons coupling with radio-frequency (RF) signal by introducing two Boltzmann relations to describe the cold and hot thermal electrons for the first time.

PACS: 52.65.Ww; 52.65.Rr; 52.50.Qt; 02.70.Bf

1. Introduction

To numerically simulate partially ionized electrical plasma, we can use the particle-in-cell (PIC) approach [1]. The ions and electrons motion are simulated by an ensemble of PIC particles. To successfully resolve the electron inertia, it will take a long time to carry out a simulation for real time duration. It is well-known that in a low-pressure partially ionized plasma at room temperature, the ions are almost never in thermal equilibrium but the electrons are generally in near-thermal equilibrium [2]. When this partially ionized plasma is saturated, an ion sheath will generate at the chamber wall and sample stage following by a pre-sheath as depicted in Fig. 1 [2]. An ion sheath is formed when a partially ionized plasma is bounded by conducting walls. In a

* Tel.: +61 2 93515972; fax: +61 2 93517726.
E-mail address: dkwok@physics.usyd.edu.au

0021-9991/$ - see front matter © 2008 Elsevier Inc. All rights reserved.
doi:10.1016/j.jcp.2008.02.005

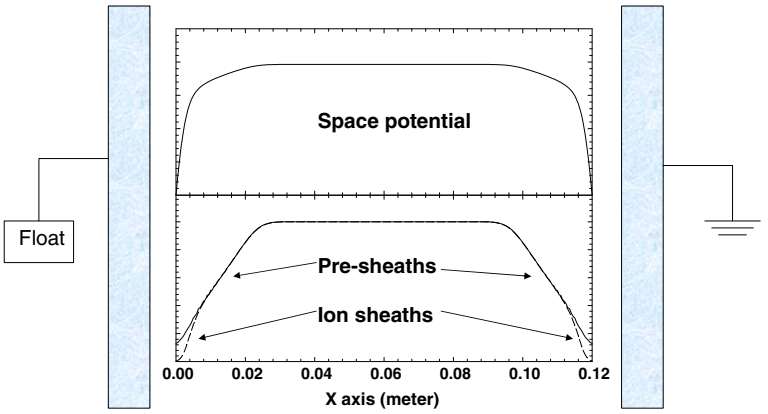

Fig. 1. A schematic of the simulation region is depicted. The left hand side of the wall is floated and the right hand side of the wall is grounded.

partially ionized plasma, the electrons are more mobile than the room temperature ions. To maintain a balanced ion and electron flux to the walls, a non-neutral positive potential region between the plasma and the walls will be formed. This positive potential region is defined as ion sheath [2]. A pre-sheath region will exist between the neutral plasma (bulk region) and non-neutral sheath region to maintain the continuity of ion flux [2]. Plasma processes such as ion implantation, ion etching, deposition, etc. happen within the ion sheaths [2]. It is not overwhelming to say that "If you know the ion sheath, you will understand the plasma process." If the electrons are in thermal equilibrium, the electron density can be written as

$$n_e(x) = n_0 \exp\left[\frac{(\phi(x) - \phi_0)}{T_e}\right] \tag{1}$$

where T_e is the electron temperature in V, and ϕ_0 is the reference potential at electron density n_0. Boltzmann distribution of electron density can be applied in the absence of electron drifts, the inertial, magnetic force and frictional force [2]. In conventional RF 13.56 MHz capacitive coupling discharges, the electron drift is zero. The electron plasma frequency at density $1 \times 10^{15}\ \mathrm{m}^{-3}$ is 285 MHz, which is much greater than the RF frequency and the electron inertial can be ignored. The electron density at the wall can be obtained from Boltzmann distribution and the lost of electrons to the walls can be estimated by the effusion flux of $1/4 n_e(x)\bar{v}$, where $n_e(x)$ is the electron density at the walls and $\bar{v}$ is the thermal velocity $\bar{v} = \sqrt{8eT_e/\pi m_e}$. In plasma immersion ion implantation, a high negative bias voltage, from a few kV to a few tens of kV, is applied to the substrate for a duration of 10–100 μs [3]. The space potential at the bulk plasma under this enormous bias voltage will nearly equal to zero. Taking the bulk plasma density as a reference point, the reference potential can be set to zero. Following the procedure of Emmert, the space potential $\phi(x)$ can be determined through a series of iteration [4]. By using the Boltzmann relation to describe electron density, the cell length and time step can be chosen to resolve the ion motion, but not necessarily small enough to resolve the electron motion. The Boltzmann relation has been used extensively in simulating plasma immersion ion implantation process with great success [4–10]. The advantage is that it will save a lot of simulation time. The cell length can be greater than electron Debye length and time step can be greater than the inverse of electron plasma frequency. The bulk plasma parameters can be obtained from analytical formula or experimental data. However, in radio-frequency (RF) coupled discharge plasma, the space potential at the bulk plasma will vary with the RF signal [2]. A lack of electron density reference with the proper potential reference makes it impossible to use Boltzmann relation in simulating RF coupled plasma.

Several approaches have been proposed to determine the reference potential ϕ_0 at reference electron density n_0. In magnetically confined low-pressure plasma, electron motion was virtually completely confined to a direction parallel to the contour surface of the magnetic field strength, which in this geometry formed concentric cylinders [11]. Electrons were treated as if they were strictly one dimensional: Axial motion and density variations were allowed, but electrons could not go from one radial annulus to another [11]. With these

approximations, Porteous et al. assumed the electrons had a Maxwell–Boltzmann distribution axially so that the electron density was represented as

$$n_e(r,z) = n_m(r)\exp\left[\frac{\phi(r,z)-\Phi(r)}{T(r)}\right] \tag{4}$$

where, $T(r)$ is the electron temperature in volt, $n_m(r)$ is the maximum electron density along a field line at a given radial position, $\Phi(r)$ is the maximum value of the self-consistent potential $\phi(r,z)$ at the radial position r [11]. In their model, the simulation of solving the Poisson's equation through successive over relation (SOR) provided the values of $N_e(r)$, the total of electrons in a finite radial annulus, $T(r)$, and $\phi(r,z)$, thus $\Phi(r)$ was obtained. Therefore, $n_m(r)$ was calculated as:

$$n_m(r) = \frac{N_e(r)}{2\pi r\Delta r\int \exp\left[\frac{\phi(r,z)-\Phi(r)}{T(r)}\right]dz} \tag{5}$$

where Δr is the width of the finite radial annulus.

However, in a lot of experimental setups, one of the electrodes can be radio-frequency (RF) powered up, and therefore, $\Phi(r)$ is not necessary self-consistent and determined. Cartwright et al. proposed a different method [12]. In their method, the reference potential was set to zero and the electron density n_0, where $\phi = 0$, will be determined. The Poisson's equation with the Boltzmann distribution of electrons was solved by Newton–Raphson iteration [12]. Poisson's equation was rewritten as

$$\delta(\phi(x)) = \nabla^2\phi(x) + \frac{e}{\varepsilon_0}\left(n_{PIC}(x) + qn_0\exp\left[\frac{-q\phi(x)}{T}\right]\right) \tag{7}$$

for full Maxwellian–Boltzmann distribution. Iteration will continue until [12],

$$\frac{\|\delta(\phi(x))\|_{L_2}}{\|\text{boundary conditions} + \rho/\varepsilon_0\|_{L_2}} \leqslant \varepsilon_{error} \tag{8}$$

where $\|\text{boundary conditions} + \rho/\varepsilon_0\|_{L_2}$ was the L_2 norm of the charge (including the Boltzmann species charge) and the boundary conditions, the known quantities in the equation. The tolerance, ε_{error}, was 1×10^{-4} n_0 was calculated as

$$n_0 = \frac{N_B}{\int_V \exp\left[\frac{-q\phi(x)}{T}\right]dx} \tag{9}$$

where N_B was the total number of Blotzmann electrons within the simulation region. It was shown that proper choice of n_0 determined whether this method was going to converge and converge to the correct solution [12].

Hagelaar et al. independently developed a similar method [13]. The non-linear Poisson's equation was generally worked around by taking the first order estimation of electron density at time $k+1$ as

$$n_e^{k+1}(x) \cong n_e^k(x)\left[1 + \frac{e}{k_B T_e}\left(\phi^{k+1}(x) - \phi^k(x)\right)\right] \tag{10}$$

which allowed the Poisson's equation to be linearized. The spatial integration was done by classical tri-diagonal algorithm. When proper time development of a discharge was included, non-physical instabilities of calculation of n_0 was observed and a stabilization term was inserted [13],

$$n_0^{k+1} = \frac{1}{p}\left[N_e^k\left(1 - \frac{q\Delta t}{p}\right) + S_{iz}V\Delta t + f\left(pn_0^k - N_e^k\right)\right] \tag{11}$$

q was the electron flux to the walls, $S_{iz}V\Delta t$ was the number of real electrons created in the volume V during one time step, N_e^k was the total number of electrons in the volume, f was an arbitrary coefficient, and p was defined as:

$$p = \int\int\int_v \exp\left[\frac{e\phi}{k_B T_e}\right]dV \tag{12}$$

Critical damping was obtained when $f = f_0 = \sqrt{q\Delta t/p}$ [13].

In these previous works, the reference potential of the Boltzmann distribution were either set to zero [12,13] or taking as the maximum potential value [11]. The reference electron density was estimated by direct Newton–Raphson method [12]. However, in plasma coupling with RF signal, the maximum potential value will vary and not necessary self-consistent. This limited the general application of Boltzmann distribution of electrons in space. Moreover, it shown that proper choice of initial reference density is essential for convergence [12] and a stabilization term was needed [13]. In this paper, a different approach to estimate the electron density reference and its proper potential reference will be developed to overcome the limitation of previous approaches. In the new approach, the electron reference density $n_{\text{ref}}(t)$ is precisely calculated. Its reference potential $\phi_{\text{ref}}(t)$ will be determined by bi-section golden rule. We will show that this approach is more robust since $n_{\text{ref}}(t)$ is precisely calculated, the tolerance criteria is well-defined, and convergence is guaranteed by applying bi-section golden rule. It is well-known in computational physics that bi-section method has a 100% successful rate in either finding a root or a minimum, i.e., the bracketed interval will decrease in size with each iteration [14]. With a well-defined tolerance criterion, the method becomes robust and stable. To increase the rate of convergence, an external loop is incorporated with the bi-section golden rule to vary the brackets.

Plasmas can show non-Maxwellian electron distributions [15]. In particular, at low-pressure (30 m Torr) RF coupled discharge plasma, it is common that the electron energy distribution function (EEDF) is bi-Maxwellian [15]. A majority of cold thermal electrons of $T_e = 0.50$ V with density of $4.2 \times 10^{15}\ \text{m}^{-3}$ mixes with a hot thermal electrons of $T_e = 3.4$ V with density of $2.0 \times 10^{14}\ \text{m}^{-3}$ [15]. Two Boltzmann distributions with different electron's temperatures and densities were analytically used to determine the floating potential of a bi-Maxwellian RF plasma and to solve the Tonks–Langmuir problem for a bi-Maxwellian plasma [16,17]. In the theoretical analysis, only averaged values of plasma potentials were calculated [17]. In situ potential variation with time has not been simulated for bi-Maxwellain electrons [17]. With the advantages of robustness and guaranteed convergence of the proposed approach, multiple Maxwellian electron distributions can be incorporated with it. The ion sheaths of a partially ionized Argon plasma contained bi-Maxwellian electrons [15] is simulated for the first time by introducing two Boltzmann relations to describe the cold and hot thermal electrons.

The paper is organized as follows. The model will be described in the next section. The model will then be validated by comparing the simulated results with a well-known analytical formula. A plasma with bi-Maxwellian electrons will be simulated by introducing two Boltzmann relations of electron density in the new approach. Finally this paper will be discussed and concluded.

2. Model

An uniform plasma is bounded by two infinite long electrodes as illustrated in Fig. 1. At time $t = 0$, the total number of electrons $N_e(0)$ is calculated by the average electron density $n_{\text{ref}}(0)$ times the length between the two walls L. In one dimension, N_e has units of m^{-2}. The electrons have a larger drifting velocity and are therefore lost to the walls much faster than the ions. At each time step, the number of electrons lost to the walls are obtained by electron flux toward the walls times the time step $\text{d}t$. The electron flux, for a full Boltzmann–Maxwellian distribution [12] is written as $1/4 n_e(x)\bar{v}$, where $n_e(x)$ is the electron density at the walls and $\bar{v}$ is the thermal velocity $\bar{v} = \sqrt{8eT_e/\pi m_e}$ [2]. For simplicity, full Boltzmann–Maxwellian distribution is used here. Other types of Boltzmann–Maxwellian distribution can be applied in the future [12]. At each time step, we obtained a new total number of electrons $N_e(t)$, i.e.,

$$N_e(t) = N_e(t - \text{d}t) - \bar{v}\text{d}t \int_{\text{walls}} \frac{1}{4} n_e(x)\text{d}x \tag{13}$$

and a new electron density reference $n_{\text{ref}}(t) = N_e(t)/L$. $n_{\text{ref}}(t)$ is unique at each time step and is independent of any iteration technique. In the proposed model, $n_{\text{ref}}(t)$ will be used to determine the reference potential in the Boltzmann relation. Since $n_{\text{ref}}(t)$ is unique, it will provide a solid indicator of convergence when finding the reference potential. By using $n_{\text{ref}}(t)$, convergence of the proposed model is unambiguous and guaranteed.

The reference potential $\phi_{\text{ref}}(t)$ of this unique $n_{\text{ref}}(t)$ will be calculated. The electron densities $n_{\text{e}}(x)$ at different position x were obtained by the Boltzmann relation,

$$n_{\text{e}}(x) = n_{\text{ref}}(t)\exp\left[\frac{(\phi(x)-\phi_{\text{ref}}(t))}{T_{\text{e}}}\right] \tag{14}$$

using $n_{\text{ref}}(t)$ from (13) with an initial guess of $\phi_{\text{ref}}(t)$. However, the value of $\phi_{\text{ref}}(t)$ is not necessary correct. To verify $\phi_{\text{ref}}(t)$, we re-calculate the electron density from $n_{\text{e}}(x)$. We defined this re-calculated electron density as $n_{\text{e,cal}}$. In one dimension coordinate, $n_{\text{e,cal}}$ is calculated as

$$n_{\text{e,cal}} = \frac{\Delta x}{L}\left[\frac{n_{\text{e}}(0)}{2} + \sum_{i=1}^{l-1} n_{\text{e}}(i\Delta x) + \frac{n_{\text{e}}(L)}{2}\right] \tag{15}$$

where Δx is the cell length. At the walls, $n_{\text{e}}(0)$ for left hand wall and $n_{\text{e}}(L)$ for right hand wall, only half the cell is in the simulation region, therefore we take half of the value calculated in Eq. (15). $n_{\text{e,cal}}$ is different from the unique $n_{\text{ref}}(t)$ because $n_{\text{e}}(x)$ is calculated with an incorrect $\phi_{\text{ref}}(t)$. The potential $\phi(x)$ is solved by Poisson equation. The Poisson equation after the substitution of the Boltzmann relation, Eq. (14), becomes

$$\nabla^2\phi(x) = -\frac{e}{\varepsilon_0}\left[Qn_i(x) - n_{\text{ref}}(t)\exp\left(\frac{(\phi(x)-\phi_{\text{ref}}(t))}{T_{\text{e}}}\right)\right] \tag{16}$$

where, Q is the charge state of the ions, e is the elementary charge, ε_0 is the electric constant, and $n_i(x)$ is the ion density. $n_i(x)$ is obtained from the PIC particle ensemble of ions. Following the procedure of Emmert [4], by iteration and relaxation, the space potential $\phi(x)$ is obtained [4,5]. The electron Boltzmann distribution can be expanded with the reference potential as

$$\begin{aligned} n(x) &= n_{\text{ref}}(t)\exp\left[\frac{\phi(x)-\phi_{\text{ref}}(t)}{T_{\text{e}}}\right] = n_{\text{ref}}(t)\exp\left[\frac{\phi(x)-\Psi(x)+\Psi(x)-\phi_{\text{ref}}(t)}{T_{\text{e}}}\right] \\ &\cong n_{\text{ref}}(t)\left[1+\frac{\phi(x)-\Psi(x)}{T_{\text{e}}}\right]\exp\left[\frac{\Psi(x)-\phi_{\text{ref}}(t)}{T_{\text{e}}}\right] \end{aligned} \tag{17}$$

The iteration stopped when the relative error of each node

$$\left|\frac{\phi_{\text{new}}(x)-\phi_{\text{old}}(x)}{\phi_{\text{old}}(x)}\right| \leqslant 1\times 10^{-6}. \tag{18}$$

After solving $\phi(x)$, $n_{\text{e}}(x)$ is calculated from Eq. (14) and $n_{\text{e,cal}}$ is calculated from Eq. (15). If the relative error between $n_{\text{e,cal}}$ and $n_{\text{ref}}(t)$, $\left|\frac{n_{\text{e,cal}}-n_{\text{ref}}}{1+n_{\text{ref}}}\right|$, is small then $\phi_{\text{ref}}(t)$ is a proper potential reference of $n_{\text{ref}}(t)$. If not, $\phi_{\text{ref}}(t)$ is re-estimated by the bi-section golden rule [14]. In bi-section golden rule, $\phi_{\text{ref}}(t)$ is bracketed by two initial values ϕ_{a} and ϕ_{b}. $n_{\text{e,cal}}$ at these two values are calculated accordingly by Eq. (15). The golden rule of bi-section shrinks the bracket down until a good estimation is obtained. $\left|\frac{n_{\text{e,cal}}-n_{\text{ref}}}{1+n_{\text{ref}}}\right|$ is the indicator in the bi-section algorithm. The procedure for finding the correct reference potential is depicted in Flow chart 1. After the appropriate reference potential $\phi_{\text{ref}}(t)$ is estimated, the electron density at different positions are calculated once again by the Boltzmann relation, Eq. (14). The electrons lost to the walls are then deducted from the total number of electrons $N_{\text{e}}(t)$ and a new average electron density $n_{\text{ref}}(t+\text{d}t)$ is calculated for the next time step. The whole procedure is repeated until the end of the simulation.

A big enough bracket is required in bi-section procedure such that the correct answer fall within it. Unfortunately, a large bracket will slow down the speed of searching the answer. To speed up the process and securing a correct answer of $\phi_{\text{ref}}(t)$, an extra loop was added on top of the standard adjustment of the bracket as depicted in Flow chart 1. Supposed we start our iteration at ϕ_{start} but the correct answer is $+10\Delta V$ away from it. After the first bi-section adjustment within the inner loop, it will return $\phi_{\text{new}} = \phi_{\text{start}} + \Delta V$. Of course the outer loop criteria will not be satisfied and the iteration will be continued until $\phi_{\text{new}} \cong \phi_{\text{start}} + 10\Delta V$. The convergence of the procedure greatly depends on the criteria of the inner bi-section loop. Since $n_{\text{ref}}(t)$ is unambig-

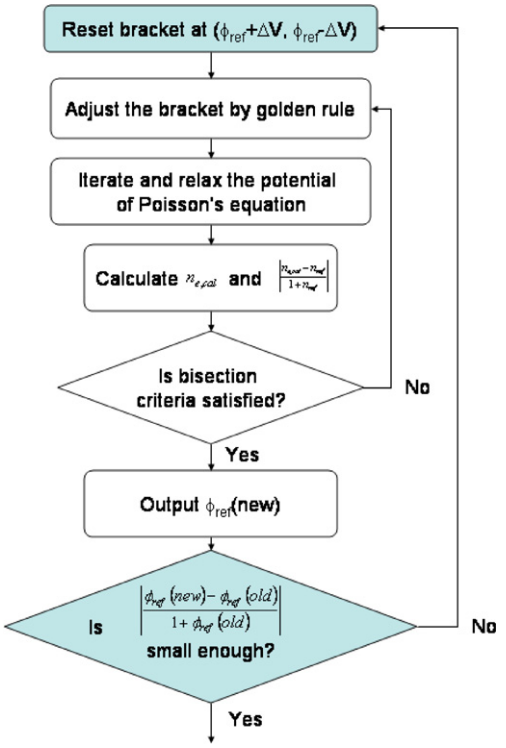

Flow chart 1. The modified procedures of estimating the referencing potential by bi-section golden rule is depicted. The convergence to the correct reference potential is guaranteed.

uous and well-defined, convergence is guaranteed in the modified method with $\left|\frac{n_{e,cal}-n_{ref}}{1+n_{ref}}\right|$ as an indicator. The proper choose of ΔV and the performance of the procedure will be discussed.

3. Validating the approach

We prove the validity of the method by comparing the simulated result with well-known analytical formula. When a partially ionized plasma is touching a floating wall, an ion sheath forms between the wall and the bulk plasma. For simplicity, the ions were assumed to be non-collisional. By balancing the ion and electron flux to the wall and setting the potential at the sheath edge as zero, the floating potential at the wall can be analytically calculated by the equation [2],

$$\Phi_w = -T_e \ln\left(\sqrt{\frac{M}{2\pi m_e}}\right) \tag{19}$$

where T_e is the electron temperature in volt, M is the ion mass, and m_e is the electron rest mass. An Argon plasma of atomic mass 40 amu and an electron temperature of 7 V will give, according to (19), a potential difference between the floating wall potential and ion sheath edge of 32.8 V. An one dimension simulation in rectangular coordinate is conducted as close to reality as possible. The left hand side wall at $x = 0.0$ representing the sample stage electrode is floating, i.e., charges will accumulate. The right hand side wall representing the chamber wall is usually grounded and the potential is set at zero. An uniform partially ionized Argon plasma of 1×10^{15} m^{-3} was initially placed between the two metal walls as depicted in Fig. 1. The ions were simulated by Particle-in-cell method [1]. The length between the two walls was 0.12 m. The region was divided into smaller cells of length = 0.5 mm. 100 PIC particles were placed in each cell giving a total of 12,000 PIC particles to simulate the ion motion. The time step was 1.0×10^{-10} s. The electrons were in thermal equilibrium with a temperature of 7 V. The surface voltage of the left hand side floating wall was determined by Gauss' law [18]. According to Gauss's law, the surface voltage of the floating wall at the next time step was calculated,

$$V_0(t+\mathrm{d}t) = V_1(t) + \frac{\sigma_c(t)\mathrm{d}x}{\varepsilon_0} \tag{20}$$

where the surface charge density $\sigma_c(t)$ was updated by the ion and electron fluxes, $\mathrm{d}x$ was the cell length, and $V_1(t)$ was the potential of the node next to the floating wall. The surface voltage $V_0(t+\mathrm{d}t)$ was substituted into Eq. (14) to estimate an electron density at the wall. Following the procedures described in Flow chart 1, a correct potential reference $\phi_{ref}(t+\mathrm{d}t)$ was obtained.

An ion sheath was formed shortly after the start of the simulation. After 3 μs of simulation, the ion sheath was established. The ion and electron densities and the space potential distributions at 5 μs were plotted in Fig. 2 near the floating wall. The ion sheath region was clearly defined between $x = 0$ and $x = 0.8$ cm, and the pre-sheath region between $x = 0.8$ cm and 3.0 cm was also observed. The region $x >= 3.0$ cm was roughly defined as the bulk plasma region. In an ideal situation starting with an uniform plasma of density $1 \times 10^{15}\ \mathrm{m}^{-3}$, the bulk plasma region shall have a density of $1 \times 10^{15}\ \mathrm{m}^{-3}$. The space potential at the bulk plasma was not zero because we had set the grounded right hand side wall as the reference potential of zero. The potential of the floating wall (left hand side wall) showed zero because the ion and electron fluxes were balanced. At the sheath edge shown in Fig. 2, the potential difference was approximately 33.5 V. Therefore, the numerically estimated potential difference between the sheath edge and floating wall fitted well with the analytical answer of 32.8 V obtained by Eq. (19). According to Bohm sheath criterion [2], the ions must gain a kinetic energy greater than or equal to $eT_e/2$, which equals 7 eV/2 = 3.5 eV in this case. The space potential at the bulk plasma was 39.27 V given the potential drop within the pre-sheath 39.3–33.5 = 5.8 V > 3.5 V. A collisionless Ar^+ ion will gain a kinetic energy of 5.8 eV when accelerated through the pre-sheath region. Therefore, the simulation did not violate the Bohm sheath criterion. For simplicity, we did not include the plasma generation in the simulation and therefore, the pre-sheath will continue extend into the bulk plasma until it hits the pre-sheath of the right hand sided wall. The plasma potential at the bulk region at $x = 6$ cm continued to gradually increased until the two pre-sheaths touched each other [19]. The plasma potential at the bulk region was plotted against run time in Fig. 3. As depicted in Fig. 3, it was shown that the pre-sheaths joined together at around 13 μs. When the two pre-sheaths joined together, the plasma starts to decay. The positive ion (space charge) density and electron density at 3, 5, 7, 10, and 15 μs were plotted in Fig. 4a. According to Child's law, the sheath edge should increase slightly as the plasma density is decreasing at constant wall potential and electron temperature. These slightly changes of the sheath edge defined as ion density = electron density was hardly observed by naked eyes. As depicted in Fig. 4b, the sheath edge did not vary much with time and almost fixed at $x = 0.85$ cm. The plasma density at the sheath edge dropped from $5.8 \times 10^{14}\ \mathrm{m}^{-3}$ at

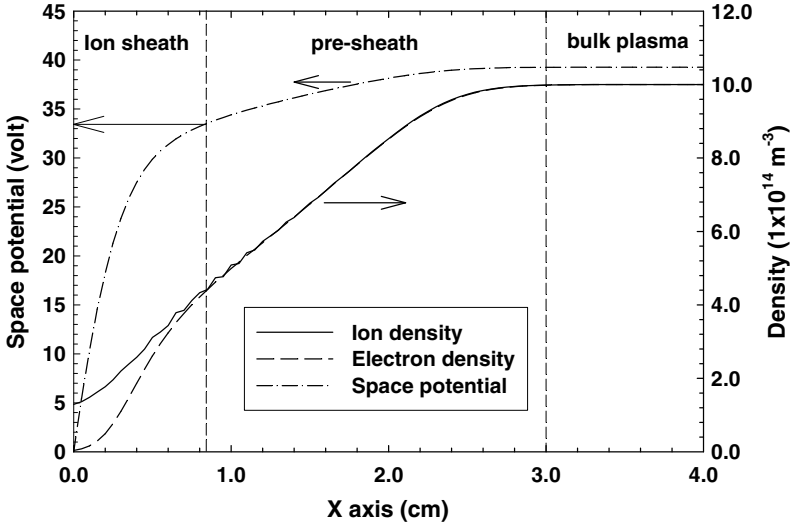

Fig. 2. The simulated space potential, ion and electron densities at the left hand side wall at 5 μs are depicted. The ion sheath, pre-sheath and bulk plasma regions are clearly defined.

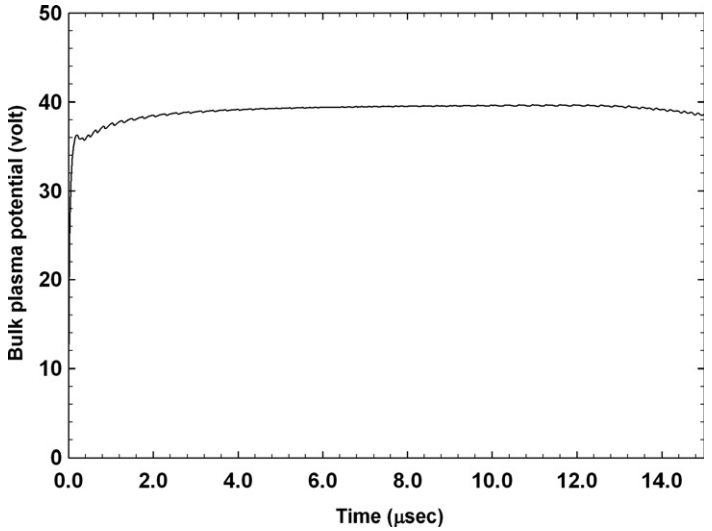

Fig. 3. The space potential at the bulk plasma at $x = 6$ cm is plotted against simulation time.

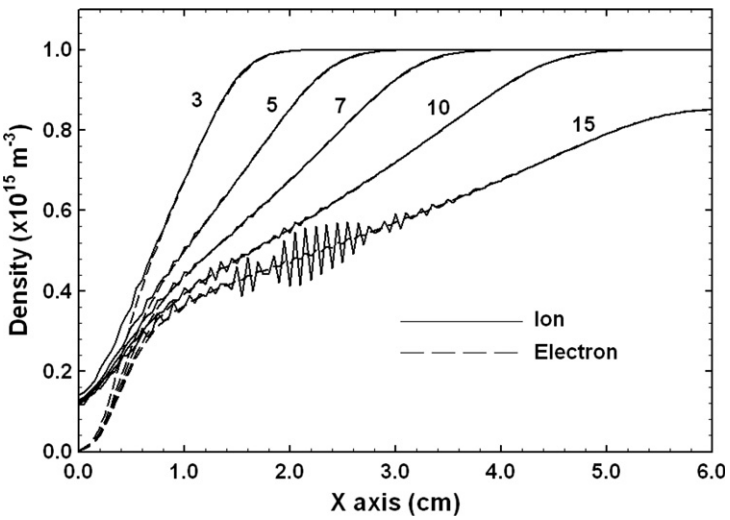

Fig. 4a. The ion and electron densities at different simulation time at the left hand side wall are depicted.

3 μs to 3.34×10^{14} m^{-3} at 15 μs [19]. Grid heating was observed after 7 μs [20–22]. The grid heating was getting worse after the two pre-sheaths joined together at 13 μs. As depicted in Fig. 3, the potential at the bulk plasma did not tremble with the grid heating. Therefore, the grid heating effect is acceptable in the simulation. The grid heating can be suppressed by jiggling the computation mesh [23]. The sheath edge data were summarized in Table 1. It showed that the ion kinetic energy acquired from the pre-sheaths region were always greater than 3.5 eV. It concluded that during the transient state of the dying plasma the kinetic energy acquired by the collisionless ions did not violate the Bohm sheath criterion. The voltage drop across the pre-sheath region were much greater than $T_e/2$, which equaled 7 V/2 = 3.5 V in this case. In an review article of Bohm criterion and sheath formation written by K–U Riemann [19], Bohm's criterion referred to the sheath edge, which was uniquely defined only in the asymptotic limit $\lambda_D/L \to 0$, where λ_D is the electron debye length and L is the all other characterize lengths of the plasma, e.g., ion mean free path. In the case of non-collision ions, zero ionization rate, and hot electrons, i.e., large λ_D, the Bohm criterion can be over-satisfied. This is essentially a matter of stationary; only in stationary situations the ion velocity equals the Bohm velocity on

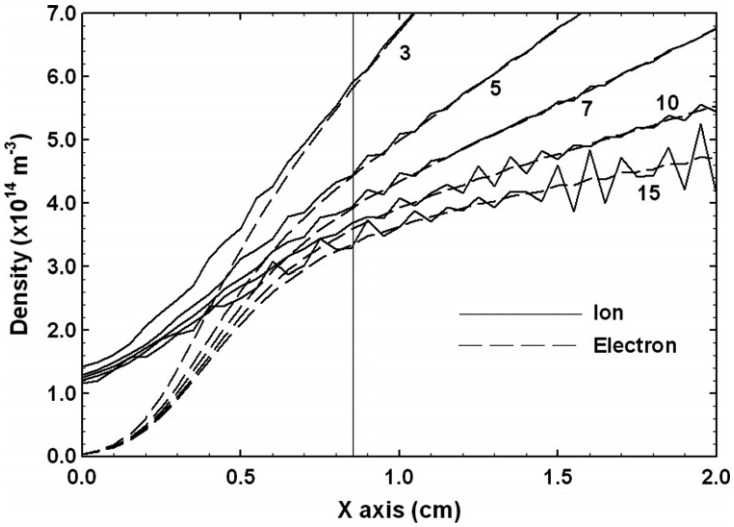

Fig. 4b. An expanded view of (a), the ion and electron densities at different simulation times at the sheath region are depicted.

Table 1
Data at different simulation time of the transient state of partially ionized Argon plasma

Time (μs)	Potential at bulk (V)	Potential at ion sheath edge (V)	Potential between bulk and ion sheath edge (V)	Electron/Ion density (10^{14} m^{-3})
3	38.9	35.1	3.8	5.80
5	39.3	33.5	5.8	4.41
7	39.5	32.9	6.6	3.91
10	39.6	32.5	7.1	3.58
15	38.6	32.1	6.5	3.34

the sheath edge. Albeit the generation of plasma has not been considered, valuable information will be achieved during the transient state before the joining of the pre-sheaths, for example, the coupling between the plasma and external matching network [24], and micro-arcing effect at the ground chamber wall [25]. In the next section, we will extend our method to simulate plasma with bi-Maxwellian electrons.

4. Multiple Boltzmann electrons

In this section, we applied the new developed method to simulate a plasma with bi-Maxwellian electrons. For simplicity, the ions are collisionless and plasma is not generated. Before we can introduce two Boltzmann relations to describe them, we have to show that there is no direct contact between these two plasma species. Electrons are mainly scattered by each other through coulomb elastic collisions [2]. The collision frequency for the cumulative effect of many collisions to produce a 90 degree deflection can be written down as [2],

$$\nu_{90} = n_g \sigma_{90} V_R \tag{21}$$

where n_g is the target particle density, σ_{90} is the scattering coefficient and $V_R = |V_1 - V_2|$ is the relative velocity in centre of mass system. σ_{90} for electron–electron scattering can be written down as

$$\sigma_{90} = \frac{8e^4}{\pi^3 \varepsilon_0^2 m_e^2 V_R^4} \ln \Lambda \tag{22}$$

Typically $\ln \Lambda = 10$ [2]. The average speeds of the cold (0.5 V) and hot (3.4 V) electrons are 4.738×10^7 and 1.235×10^8 cm s^{-1}, respectively. The collision frequency of the cold electrons by the hot electrons is 1.4221×10^4 Hz and the collision frequency of the hot electrons by the cold electrons is 2.4887×10^5 Hz. They are very low when compared to the effective frequency for momentum transfer between electrons and argon

neutrals [26]. At 30 m Torr, the collision frequency between electrons and background Argon gas in the range between 1 and 10 V is $5.3 \times 10^9 \times 30 \times 10^{-3} = 1.59 \times 10^8$ Hz [26]. In other words, the electrons, no matter whether they are cold or hot, will not reach thermal equilibrium by scattering with each other but they will separately reach equilibrium by scattering between neutrals, for example argon atoms. There will be interaction/exchange between the hot and cold electrons through the Ar intermediates. However, the main lost of these electrons are due to diffusion to the sample stage and chamber wall. The create/destroy rates of electrons due to interaction through Ar intermediates can be ignored. Therefore, it is theoretically correct to treat the cold and hot electrons as two different plasma species and use two Boltzmann relations to describe them. After substituting the two Boltzmann relations into the Poisson equation, it becomes

$$\nabla^2\phi(x) = -\frac{e}{\varepsilon_0}\left[Qn_i(x) - n_{\mathrm{ref}}^{\mathrm{hot}}(t)\exp\left(\frac{e\left(\phi(x)-\phi_{\mathrm{e}}^{\mathrm{hot}}\right)}{T_{\mathrm{e}}^{\mathrm{hot}}}\right) - n_{\mathrm{ref}}^{\mathrm{cold}}(t)\exp\left(\frac{e\left(\phi(x)-\phi_{\mathrm{e}}^{\mathrm{cold}}\right)}{T_{\mathrm{e}}^{\mathrm{cold}}}\right)\right] \tag{23}$$

Eq. (23) can be expanded by the Emmert procedure [4] except in this case, we have two referencing potentials to be estimated. Bi-section golden rules will be separately applied to these two electron species until the reference potentials have converged and relaxed as depicted in Flow chart 2. As shown in Flow chart 2, separated golden rules are applied to estimate the referencing potentials of hot and cold electrons. However, a new relaxed space potential (at each node) will no doubt change the electron densities for both species. To make sure that the hot and cold reference potentials have converged, the exit criteria are checked together at the end. In the simulation, the length between the two walls was 0.12 m. An RF (13.56 MHz) signal of amplitude 150 V was applied to the right hand side wall and the left hand side wall was grounded. The cell length was 0.5 mm and the time step was one RF cycle divided by 200, which equaled to 3.7×10^{-10} s. After 2 μs of simulation, two ion sheaths were established at the walls. The potential variations within 1 RF cycle at 5 μs were plotted in Fig. 5a. As depicted in Fig. 5a, the potential at the left hand side wall was always zero because it was

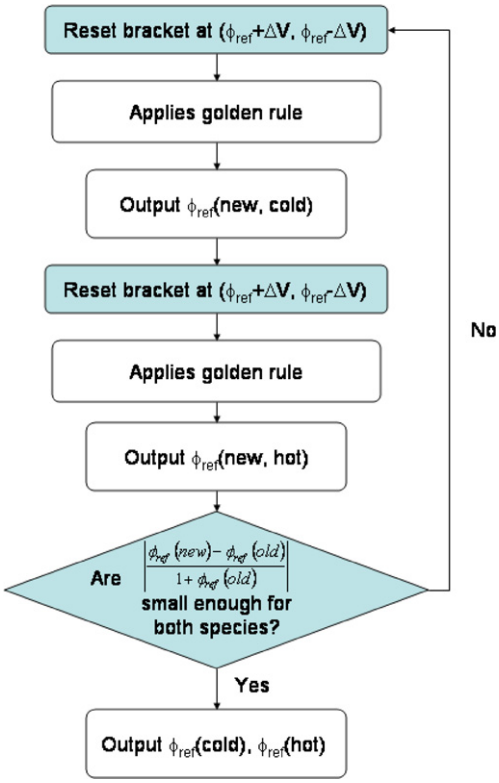

Flow chart 2. The procedures of estimating the referencing potentials of the two Boltzmann distributions by the modified bi-section golden rule is depicted.

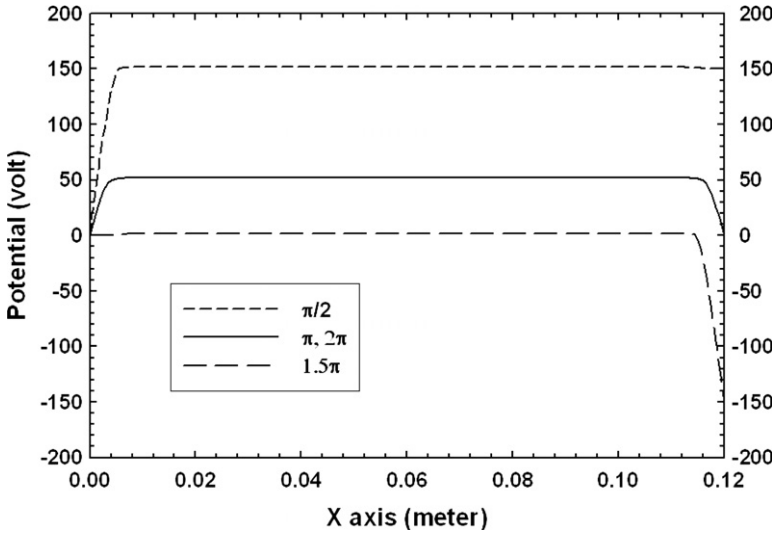

Fig. 5a. The simulated space potential distributions of the RF cycle at phase $\pi/2$, π, 1.5π, and 2π at 5 μs are depicted. The applied voltage is given by $V(x = 0.12\text{ m}) = 150 \times \sin(\omega t)$. The space potential at the bulk plasma never drops below zero.

grounded. The right hand side wall potential varied with the RF signal. It was maximum of +150 V at phase of $\pi/2$, at minimum of −150 V at phase of 1.5π, and zero at phases of π and 2π. The space potential in the bulk plasma varied with the RF cycle but would never drop below zero voltage because the total positive space charges were bigger than the negative space charges. It is because the electrons lost to the walls much faster than the ions. The ion and electron densities within one RF cycle at 5 μs were plotted in Fig. 5b. The density profiles at both walls were enlarged. The heavy ions only responded to the average electric field and therefore did not change in one RF cycle at all. On the other hand, the light electrons responded instantaneously with electric field. At the phase of $\pi/2$, the right hand side wall had a potential of +150 V and the ion sheath was nearly vanished. On the other hand, the left hand side wall has a relatively speaking negative potential with respect to the bulk plasma and therefore, a thick ion sheath was formed. At the phase of 1.5π, the right hand

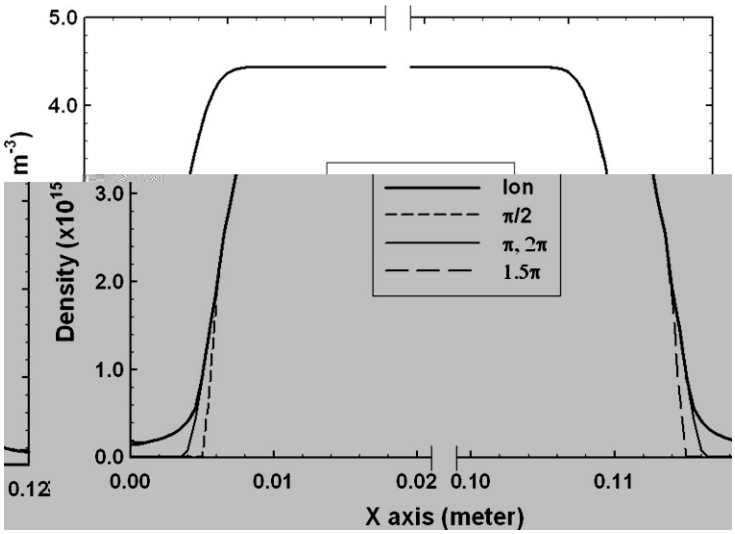

Fig. 5b. The simulated ion and electron densities distributions of the RF cycle at phase $\pi/2$, π, 1.5π, and 2π at 5 μs are depicted. The sheath regions at the left and right hand side wall are enlarged. The heavy ions density in solid thick line did not response simultaneously with the RF signal.

side wall had a potential of −150 V and therefore, a thick ion sheath was created. In contrast, the ion sheath was nearly vanished on the left hand side wall. The ion density profile did not decay exponentially in the ion sheath region of a plasma with bi-Maxwellian electrons as depicted in Fig. 5b. An elongated tail of low ion density was extended from the sheath edge to the wall. This extended tail was generated by the small population of hot electrons. Presumably, the ion sheath, especially in the negative RF cycle, forms a potential barrier for the electrons. The hot electrons with a higher mean speed can penetrate deeper into the ion sheath. After counterbalance with the ion flux, the ion density profile shows non-exponential profile. A discharge emission spectrum experimentally revealed a non-exponential of light intensity within the ion sheath region at 90 m Torr RF discharged Ar plasma [27]. It shows that the simulation of the transient state of the partially ionized plasma with bi-Maxwellian electrons has reproduced the main feature, measured by emission spectroscopy, in the ion sheath regions coupling with RF signal.

5. Discussion

5.1. Time step

Two time steps were used in the simulations. A time step of 1.0×10^{-10} s was applied to simulate the Argon plasma with a Maxwellian electron of temperature 7 V. As depicted in Fig. 3, the maximum plasma potential was about 40 V during the simulation. Therefore, the maximum kinetic energy of an Argon ion acquired from the ion sheath is 40 eV. A 40 eV Argon ion will have a velocity of 1.38×10^4 ms^{-1}. In 1.0×10^{-10} s, the Argon ion can travel a distance of 1.36×10^{-6} m that is much less than the cell length of 0.5 mm. A time step of 1.0×10^{-10} s is accurate to simulate this plasma system. By describing the electron density through Boltzmann relation, the cell length and time step are not necessarily small enough to resolve the electron motion.

In the Argon plasma with bi-Maxwellian electrons, one of the electrodes was powered by a RF signal of amplitude 150 V. The time step was one RF cycle, 7.37×10^{-8} s, divided by 200, which equaled to 3.7×10^{-10} s. The plasma potential will vary with the RF signal. As depicted in Fig. 5a, the maximum plasma potential is around 150 V and the maximum kinetic energy an Argon ion can be acquired from the ion sheath is 150 eV. A 150 eV Argon ion will have a velocity of 2.68×10^4 ms^{-1}. In 3.7×10^{-10} s, the Argon ion can travel a distance of 1.0×10^{-5} m that is 50 times less than the cell length of 0.5 mm. Therefore, a time step of 3.7×10^{-10} s is accurate enough to simulate Argon plasma with bi-Maxwellian electrons.

5.2. Bi-section bracket

In a time step, intensive computational steps will be conducted within the procedure of seeking the correct reference potential through the bi-section golden rule. As mentioned in section model, a big enough bracket was required in bi-section procedure such that the correct answer fall within it. However, a large bracket will take a long time to sink the bracket to the correct answer. An extra loop was added on top of the standard adjustment of the bracket to speed up the searching. In this section, the size of the bracket ΔV in Flow charts 1 and 2 will be systematically investigated on the efficiency of searching the correct reference potential $\phi_{\text{ref}}(t)$ at time t.

An Argon plasma with bi-Maxwellian electrons, a majority of cold thermal electrons of $T_e = 0.50$ V with density of 4.2×10^{15} m^{-3} and a hot thermal electrons of $T_e = 3.4$ V with density of 2.0×10^{14} m^{-3}, is used in the investigation. The Argon plasma is bounded by two electrodes separated by 0.12 m. The cell size is 0.5 mm and the time step is fixed at 3.7×10^{-10} s. At each time step, the simulation will go through the procedure of seeking correct reference potentials for the hot and cold electron species as depicted in Flow chart 2. The procedures depicted in Flow chart 2 consisted of several while loops nesting together. We define the outmost loop of setting the bracket as "ref. loop". When bi-section golden rule is applied, it will take several steps/loops before the bracket will be reduced smaller than the existing criteria and jumped out the golden rule. We define the step taken within the bi-section golden rule section as "golden loop". The core activity within the golden loop is to iterate the potential of each node by applying successive over relation (SOR). We define a round of iterating the total of 241 nodes as an "iterate loop". It usually takes many iterate loops before the potential of each single node to be relaxed. The efficiency of the procedure depicted in Flow chart 2 is analyzed by plotting

the number of ref. loop, golden loop, and iterate loop against the run time. Three ΔV of 1 V, 3 V, and 5 V are used in the analysis. Two boundary conditions will be applied, i.e., the electrodes are grounded, and one of the electrodes is RF powered with an amplitude of 150 V.

Fig. 6 plotted the number of ref. loop (a), golden loop (b), and iterate loop (c) against the simulation time when the electrodes were grounded. As shown in Fig. 6a, after the established of ion sheaths at the electrodes, the program spent around 1–2 ref. loops to obtain the reference potentials. There is no significant difference

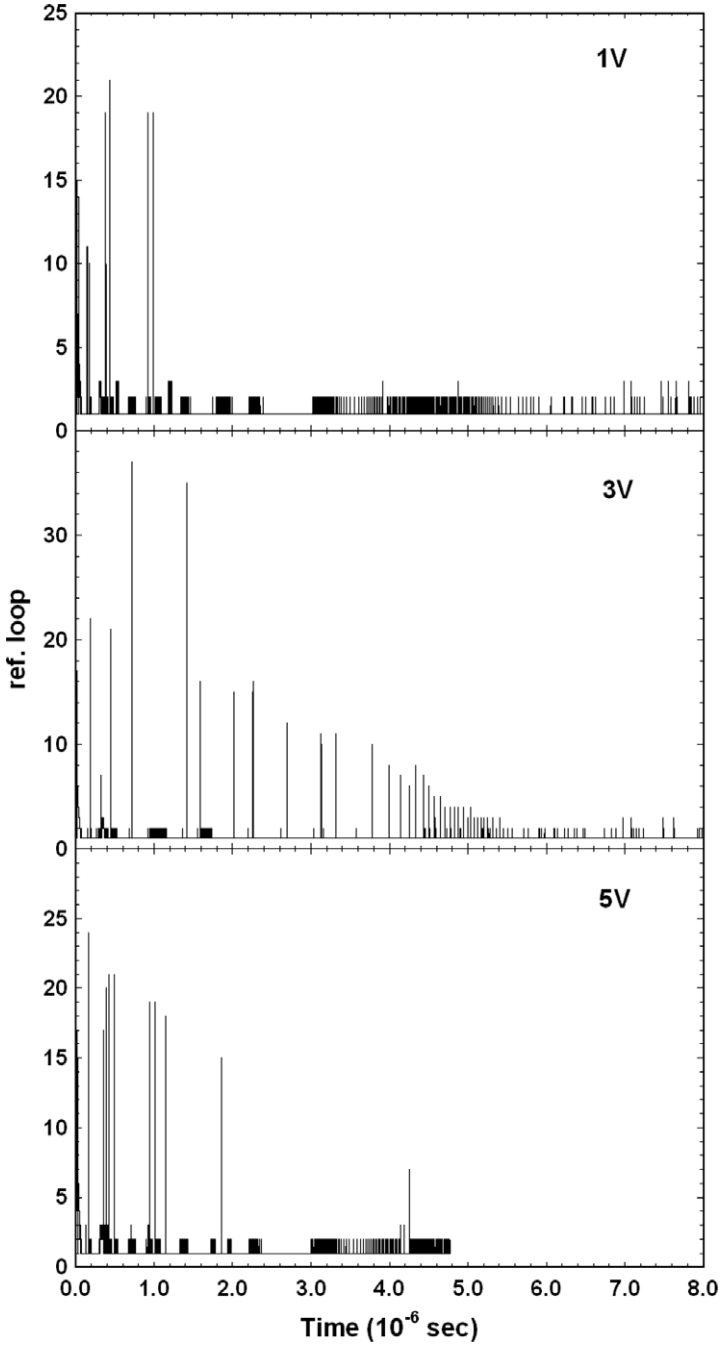

Fig. 6a. The number of ref. loop was plotted against run time when $\Delta V = 1$ V, 3 V, and 5 V. The electrodes were grounded.

between $\Delta V = 1$ V, 3 V, and 5 V. However, the simulation stopped at 4.8×10^{-6} s when $\Delta V = 5$ V. The tolerance $\left|\frac{n_{e,cal} - n_{ref}}{1 + n_{ref}}\right|$ went to infinity. During the inner golden bi-section loop for the cold electrons of Flow chart 2, the Boltzmann term of the hot electron species will be re-calculated by Eq. (23). With a large ΔV of 5 V, the Boltzmann term became unreasonable large and caused the tolerance went to infinity. Fig. 6b depicted the number of golden loop against simulation time. After the established of ion sheaths, the program spent in

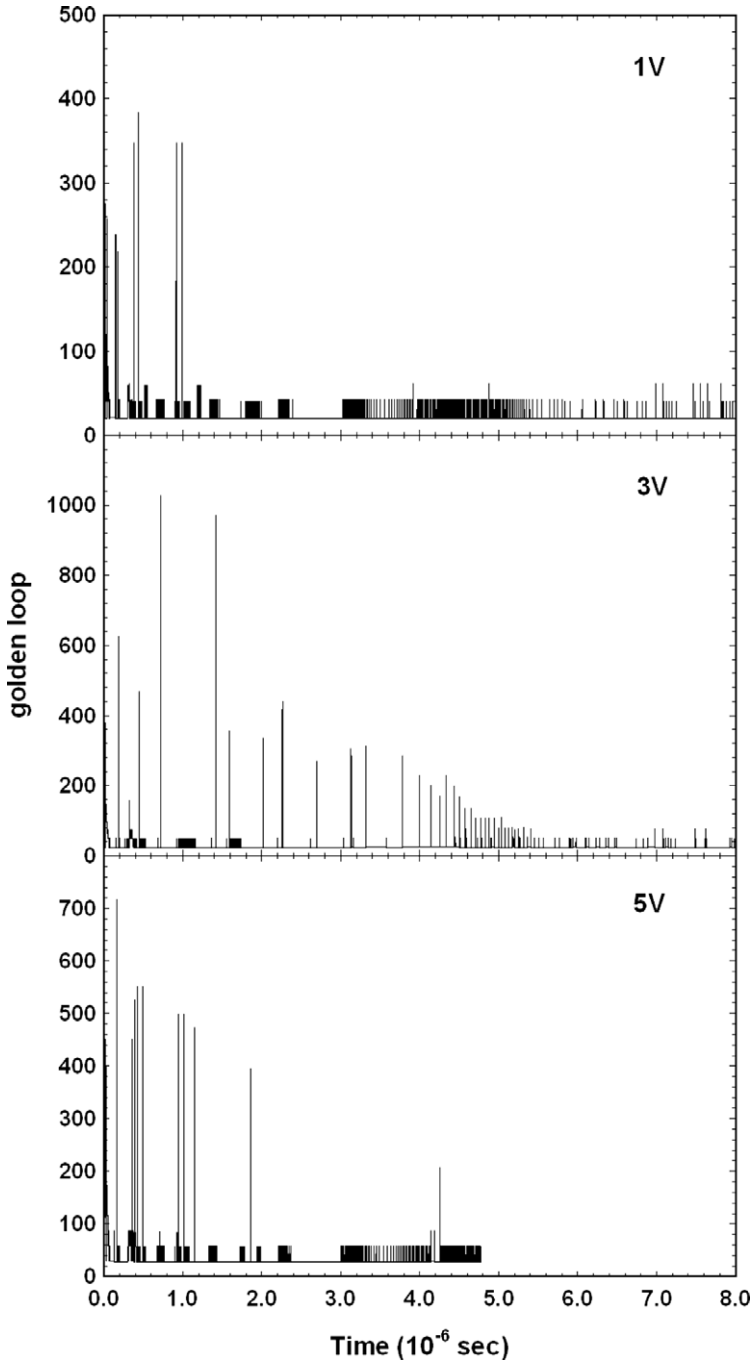

Fig. 6b. The number of golden loop was plotted against run time when $\Delta V = 1$ V, 3 V, and 5 V. The electrodes were grounded.

average 20 golden loops when $\Delta V = 1$ V, 24 loops when $\Delta V = 3$ V, and 28 loops when $\Delta V = 5$ V. It is normal for bi-section golden rule because it takes more turns to sink down a larger bracket. Fig. 6c depicted the number of iterate loop against simulation time. As shown in Fig. 6c, there is significant difference of applying a larger ΔV. After the established of ion sheaths, the program spent in average 300 loops when $\Delta V = 1$ V, 684 loops when $\Delta V = 3$ V, and 2170 loops when $\Delta V = 5$ V. The increase in computational workload is non-linear because the Poisson's equation with the Boltzmann distribution term is non-linear. The non-linear

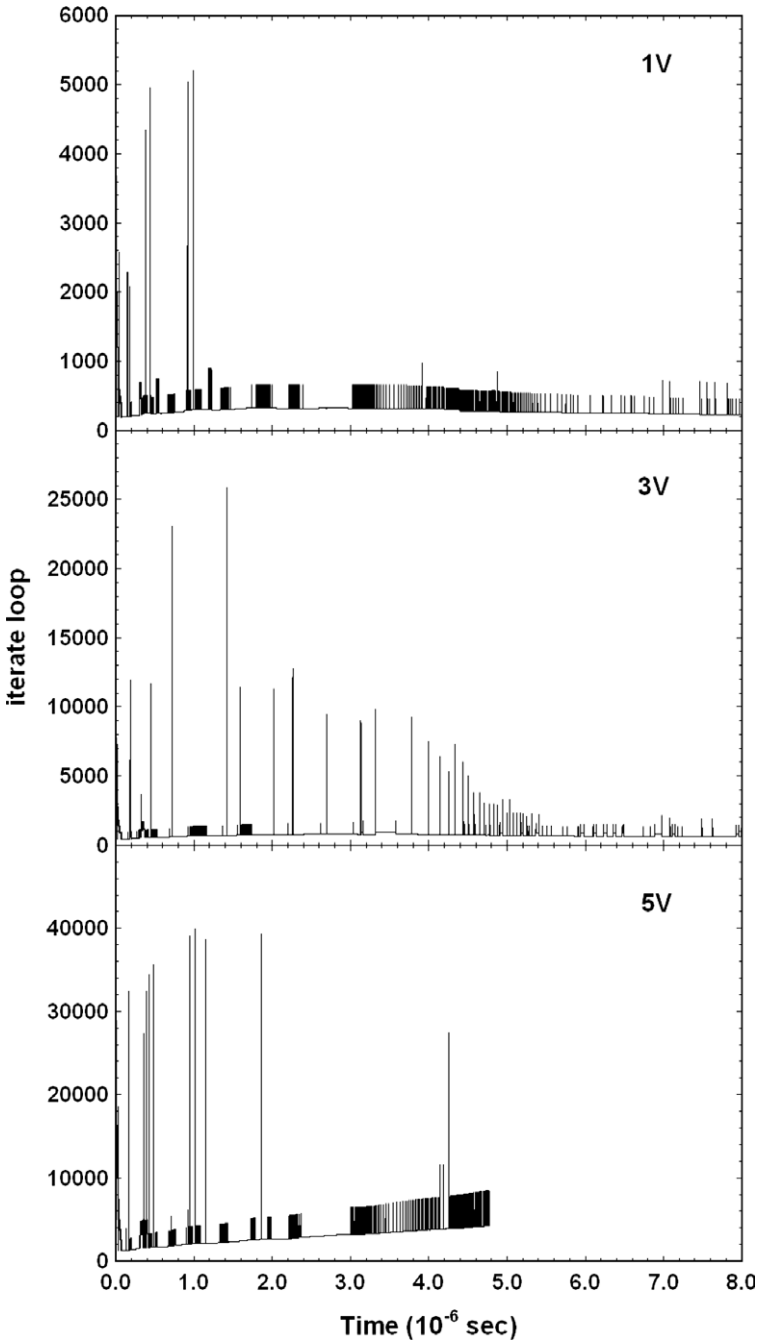

Fig. 6c. The number of iterate loop was plotted against run time when $\Delta V = 1$ V, 3 V, and 5 V. The electrodes were grounded.

Poisson's equation with the Boltzmann distribution term was expanded by Emmert method of Eq. (15). In golden bi-section rule, the reference potential bounced forward and backward within the bracket. The exponential terms of Eq. (16) became very large and it took more iterations to successive over relax the potential. A smaller ΔV speeded up the simulation.

Fig. 7 plotted the number of ref. loop (a), golden loop (b), and iterate loop (c) against the run time when one of the electrodes was powered by an RF (13.56 MHz) signal of amplitude 150 V. The plasma potential was

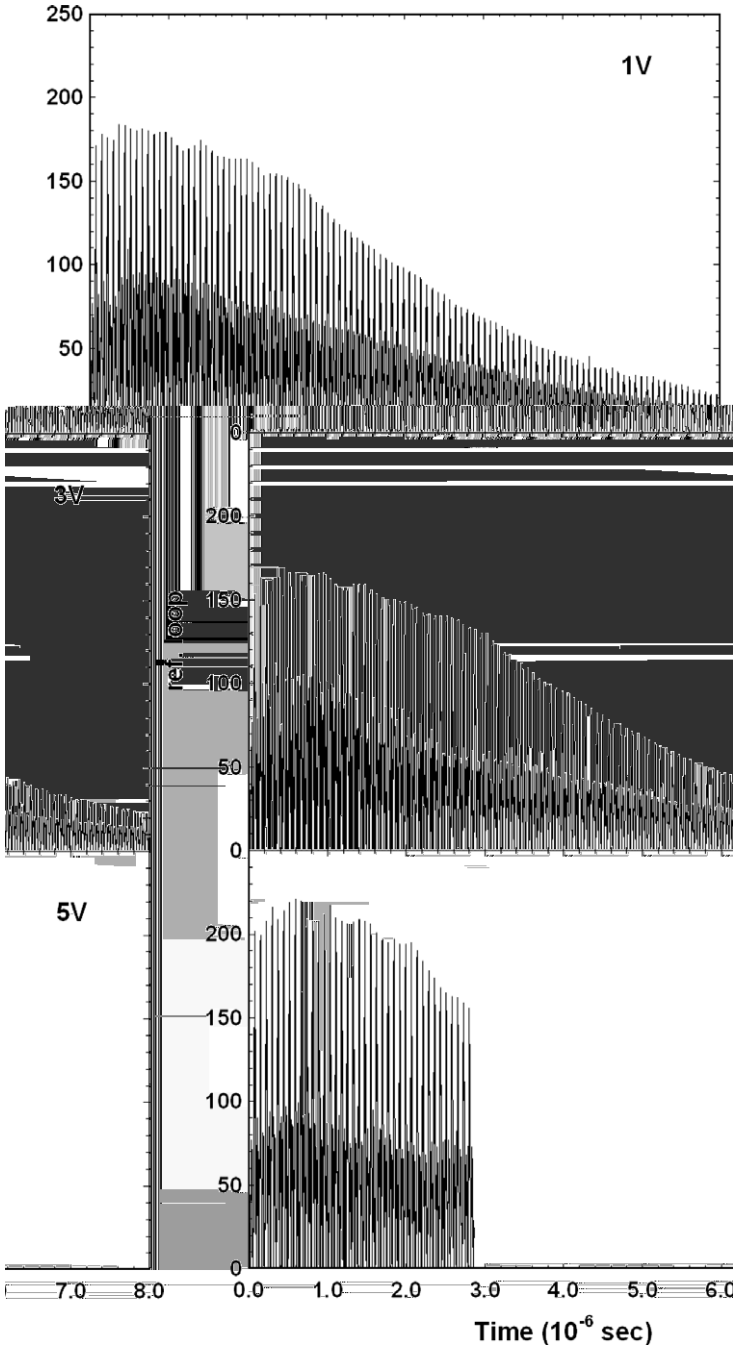

Fig. 7a. The number of ref. loop was plotted against run time when $\Delta V = 1$ V, 3 V, and 5 V. One of the electrodes were RF (13.56 MHz) powered of amplitude 150 V.

varied with the RF signal and the number of loops spent by the program greatly depended on the phase of the RF signal. When the RF signal was on its maximum or minimum, i.e., 0.5π and 1.5π in Fig. 5, the program spent less iterations to successive over relax the potentials because the plasma potential varied a little with time step. On the other hand, when the RF signal was 1π and 2π in Fig. 5, the program spent a lot of iterations to successive over relax the potentials because the plasma potential varied a great amount with time step. There-

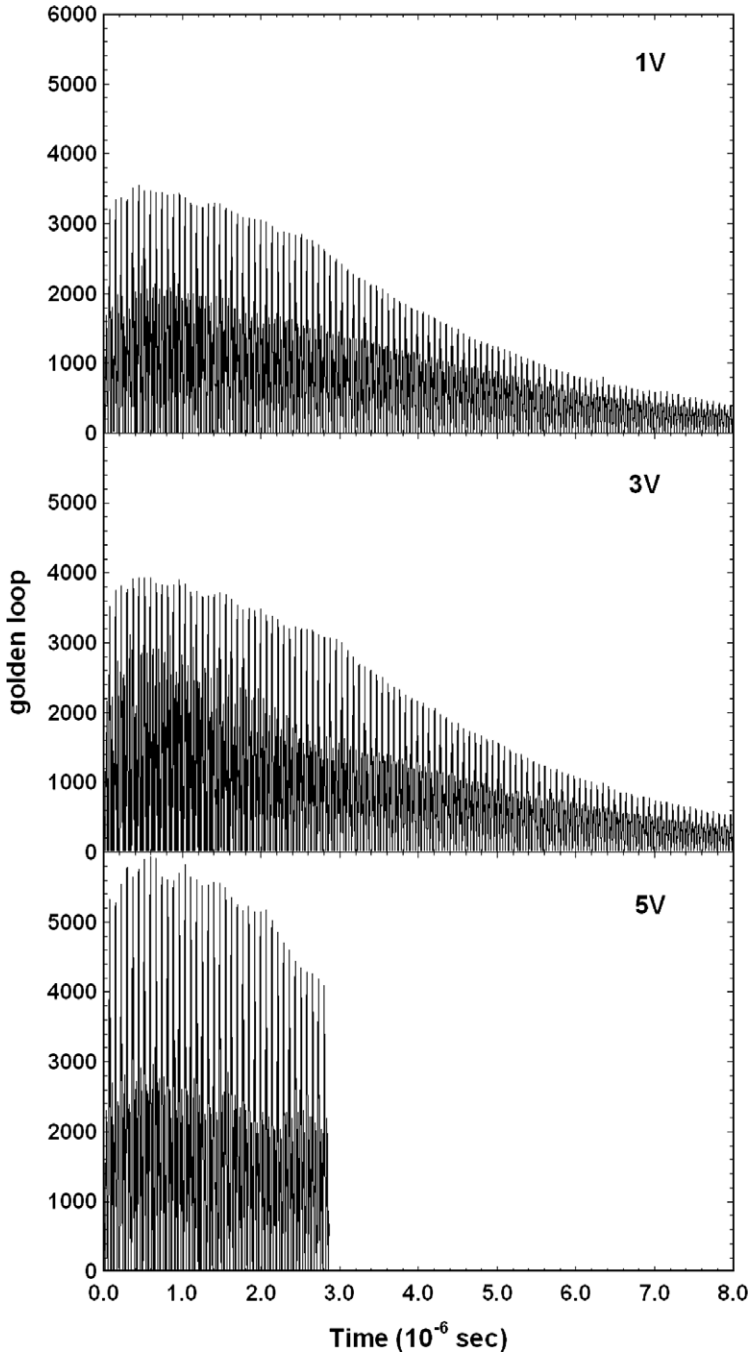

Fig. 7b. The number of golden loop was plotted against run time when $\Delta V = 1$ V, 3 V, and 5 V. One of the electrodes were RF (13.56 MHz) powered of amplitude 150 V.

fore, the number of loops spent by the program cycled with the simulation time as depicted in Fig. 7. When the ion sheaths were established, the program spent less loops on iterating the potentials. A larger ΔV in general caused more loops to be spent on iteration. The simulation stopped at 2.9×10^{-6} s when $\Delta V = 5$ V because the tolerance $\left|\frac{n_{e,cal} - n_{ref}}{1+n_{ref}}\right|$ went to infinity.

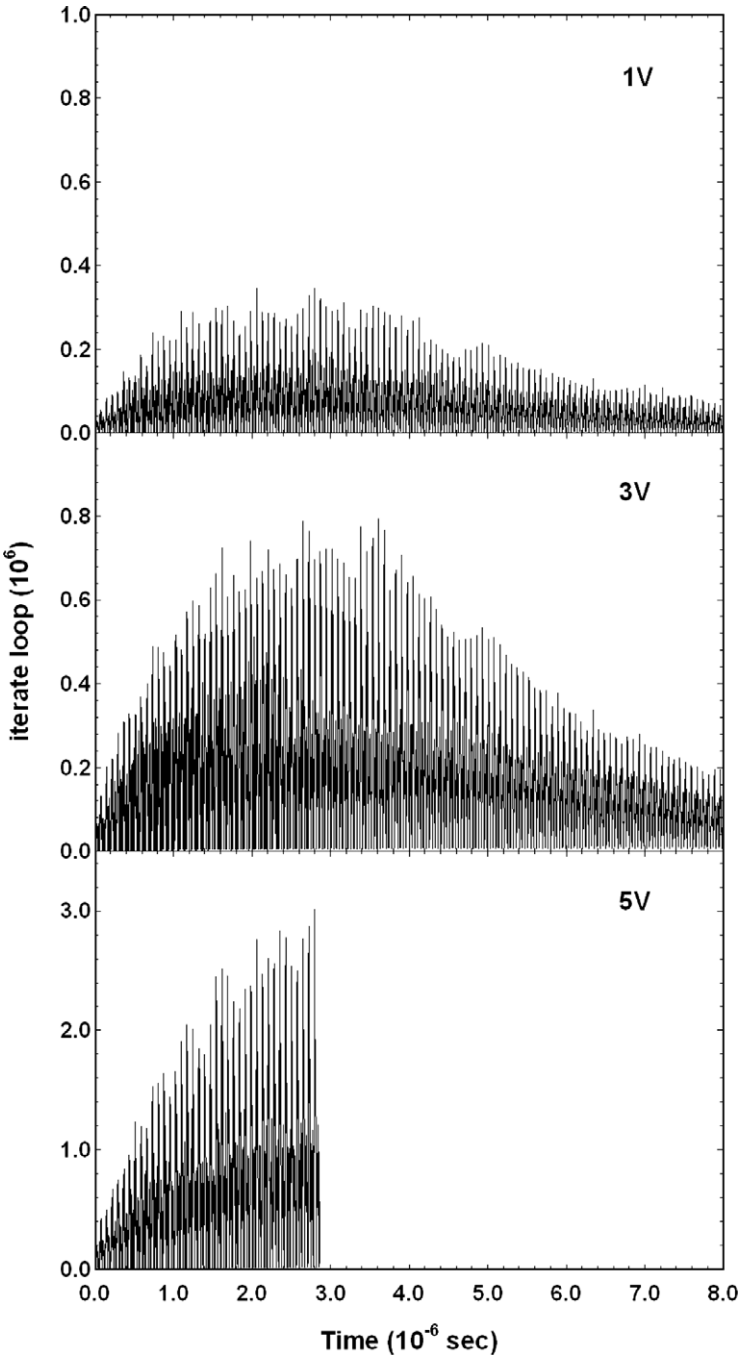

Fig. 7c. The number of iterate loop was plotted against run time when $\Delta V = 1$ V, 3 V, and 5 V. One of the electrodes were RF (13.56 MHz) powered of amplitude 150 V.

6. Conclusion

A robust and stable numerical algorithm was developed for the hybrid method of particle-in-cell ions and Boltzmann distribution of electrons. A different approach to estimate the electron density reference and its proper potential reference was developed to overcome the problems of instability and divergence of previous approaches. The electron density reference was precisely calculated, the tolerance criterion was well-defined, and convergence was guaranteed by applying bi-section golden rule. To increase the rate of convergence, an external loop was incorporated with the bi-section golden rule to vary the brackets. The approach was proved by comparing the simulated result with well-known analytical formula. The simulated sheath potential at a floating wall was close to the analytical result. The collisionless ion kinetic energy acquired from the voltage difference between the pre-sheath and ion sheath did not violate the Bohm sheath criterion. For work that focuses on the plasma process at the ion sheath and not on the generation of plasma, this method saves a lot of simulation time by avoiding time consuming particle or kinetic model of electrons.

An external loop was introduced to vary the bracket incorporating with the bi-section golden rule in Flow chart 1. This external loop only worked with a well-defined tolerance criterion. It showed that a small bracket size ΔV speeded up the simulation without decreasing the accuracy. The accuracy of the simulation depended mainly on the time step and cell size. A small bracket size was also necessary in simulating plasma with multiple Boltzmann distributions electrons. It showed that a large ΔV of 5 V caused the tolerance went to infinity. A small ΔV will stabilize the iteration process.

This work clearly showed that Boltzmann relation can be applied to simulate the transient states of a partially ionized plasma with an expanding sheath towards an uniform bulk plasma. In a review article on sheath formation [19], in the asymptotic limit $\lambda_D/L \to 0$, a transition layer is needed between the pre-sheath and sheath region. The used of Boltzmann relation in the simulation can provide important information of this transition layer in the ideal/close-to-ideal case.

The aim of the paper is to demonstrate and validate the new approach. For simplicity, the ions were collisionless and plasma was not generated, i.e., only transient state of ion sheaths were simulated. The advantage of simulating a transient state is that result can be generated in a short period of time. MCC–PIC model will be included to simulate the collisional ions and generation of plasma [28]. The PIC electrons will be incorporated with Boltzmann electrons for generation of plasma [12].

We have used the new approach to simulate the ion sheaths locations of a plasma with bi-Maxwellian electrons within an RF cycle by introducing two Boltzmann relations to describe the cold and hot thermal electrons in an RF coupled partially ionized Argon plasma for the first time. The numerical method was successfully applied to simulate a semi-transparent conducting mesh electrode for plasma immersion ion implantation [29], enhancement of micro-arcing at a grounded chamber wall in a radio-frequency capacitive discharged plasma [25], and RF coupling of an partially ionized plasma with an auto-matching network [24].

Acknowledgement

The author would like to acknowledge Yongbai Yin, Micheal Proschek, A.A. Samarian, and Christophe Cornet of the Applied and Plasma Physics Group, School of Physics, University of Sydney, NSW 2006, Australia, for their kind discussions of the work. The author would also like to acknowledge the reviewers for their useful comments and kind revision of the manuscript. The author is supported by the Denison Fellowship of the School of Physics, University of Sydney.

References

[1] C.K. Birdsall, A.B. Langdon, Plasma Physics via Computer Simulation, McGraw-Hill, New York, 1991.
[2] M.A. Lieberman, A.J. Lichtenberg, Principles of Plasma Discharges and Materials Processing, John Wiley and Sons, New York, 1994.
[3] P.K. Chu, S. Qin, C. Chan, N.W. Cheung, L.A. Larson, Plasma immersion ion implantation – a fledgling technique for semiconductor processing, Mater. Sci. Eng. R: Reports R 17 (6–7) (1996) 207–280.
[4] G.A. Emmert, M.A. Henry, Numerical simulation of plasma sheath expansion, with applications to plasma-source ion implantation, J. Appl. Phys. 71 (1992) 113–117.

[5] X.C. Zeng, T.K. Kwok, A.G. Liu, P.K. Chu, B.Y. Tang, Plasma immersion ion implantation of the interior surface of a large cylindrical bore using an auxiliary electrode, J. Appl. Phys. 83 (1998) 44–49.
[6] X.C. Zeng, T.K. Kwok, A.G. Liu, P.K. Chu, B.Y. Tang, Transient sheath in a small cylindrical bore with an auxiliary electrode for finite-rise-time voltage pulses, IEEE Conference Record – Abstracts, 1997 IEEE International Conference on Plasma Science (Cat. No. 97CH36085), IEEE, 1997, pp. 215–16.
[7] D.T.K. Kwok, P.K. Chu, C. Chung, Profile control in BF/sub 3/plasma doping, J. Appl. Phys. 88 (2000) 3198–3201.
[8] D.T.K. Kwok, R.K.Y. Fu, P.K. Chu, Two-dimensional particle-in-cell plasma immersion ion implantation simulation of gear/windmill geometry in cylindrical co-ordinates along the (*r*-theta) plane, Elsevier Surface Coat. Technol. 156 (2002) 97–102.
[9] D.T.K. Kwok, M.M.M. Bilek, D.R. McKenzie, P.K. Chu, The importance of bias pulse rise time for determining shallow implanted dose in plasma immersion ion implantation, Appl. Phys. Lett. 82 (2003) 1827–1829.
[10] D.T.K. Kwok, M.M.M. Bilek, D.R. McKenzie, T.W.H. Oates, P.K. Chu, Disturbance of a Langmuir probe at the steady-state sheath boundary in a drifting plasma, IEEE Trans. Plasma Sci. 32 (2004) 422–428.
[11] R.K. Porteous, D.B. Graves, Modeling and simulation of magnetically confined low-pressure plasmas in two dimensions, IEEE Trans. Plasma Sci. 19 (1991) 204–213.
[12] K.L. Cartwright, J.P. Verboncoeur, C.K. Birdsall, Nonlinear hybrid Boltzmann-particle-in-cell acceleration algorithm, Phys. Plasmas 7 (2000) 3252–3264.
[13] G.J.M. Hagelaar, How to normalize Maxwell–Boltzmann electrons in transient plasma models, J. Comput. Phys. 227 (2007) 871–876.
[14] P.L. DeVries, A First Course in Computational Physics, Wiley, New York, 1994.
[15] V.A. Godyak, R.B. Piejak, B.M. Alexandrovich, Probe diagnostics of non-Maxwellian plasmas, J. Appl. Phys. 73 (1993) 3657–3663.
[16] V.A. Godyak, V.P. Meytlis, H.R. Strauss, Tonks–Langmuir problem for a bi-Maxwellian plasma, IEEE Trans. Plasma Sci. 23 (1995) 728–734.
[17] F.A. Haas, N. Braithwaite, Floating potential in a bi-Maxwellian RF plasma, J. Phys. D: Appl. Phys. 35 (2002) 303–306.
[18] W.J. Duffin, Electricity and Magnetism, McGraw-Hill, London, 1980.
[19] K.U. Riemann, The Bohm criterion and sheath formation, J. Phys. D: Appl. Phys. 24 (1991) 493–518.
[20] H. Ueda, Y. Omura, H. Matsumoto, T. Okuzawa, A study of the numerical heating in electrostatic particle simulations, Comput. Phys. Commun. 79 (1994) 249–259.
[21] P.W. Rambo, Numerical heating in hybrid plasma simulations, J. Comput. Phys. 133 (1997) 173–180.
[22] C.K. Birdsall, N. Maron, Plasma self-heating and saturation due to numerical instabilities, J. Comput. Phys. 36 (1980) 1–19.
[23] J.U. Brackbill, G. Lapenta, A method to suppress the finite-grid instability in plasma simulations, J. Comput. Phys. 114 (1994) 77–84.
[24] D.T.K. Kwok, A Phasor-particle model for coupling between an auto-matching network and electrical plasma in radio-frequency capacitive discharged system, J. Appl. Phys. 100 (2006) 063306.
[25] D.T.K. Kwok, Y.B. Yin, M.M.M. Bilek, D.R. McKenzie, Enhancement of micro-arcing at a grounded chamber wall by non-vanishing ion sheath in a radio-frequency capacitive discharged plasma, Appl. Phys. Lett. 87 (2005) 181501–181503.
[26] Y.P. Raizer, Gas Discharge Physics, Springer-Verlag, Berlin, 1991.
[27] A.A. Samarian, B.W. James, Sheath measurement in RF-discharge plasma with dust grains, Phys. Lett. A 287 (2001) 125–130.
[28] V. Vahedi, M. Surendra, A Monte Carlo collision model for the particle-in-cell method: applications to argon and oxygen discharges, Comput. Phys. Commun. 87 (1995) 179–198.
[29] R.C. Powles, D.T.K. Kwok, D.R. McKenzie, M.M.M. Bilek, Simulation of a semi-transparent conducting mesh electrode for plasma immersion ion implantation, Phys. Plasmas 12 (2005) 93507-1–93507-6.